AIChE

Compressible and Incompressible 1-D Linear Wave Propagation Assessment in Fast Fluidized Beds

J. R. G. Sánchez-López and A. Soria
Group of Interfacial and Multiphase Systems, Chemical Engineering, I.P.H. Department, Universidad Autónoma Metropolitana-Iztapalapa, Col. Vicentina, México, D. F., 09340, Mexico

E. Salinas-Rodríguez
Group of Process Systems Engineering and Complex Fluids, Energy Resources Engineering, I.P.H. Department, Universidad Autónoma Metropolitana-Iztapalapa, Col. Vicentina, México, D. F., 09340, Mexico

DOI 10.1002/aic.12521
Published online February 15, 2011 in Wiley Online Library (wileyonlinelibrary.com).

We propose two equivalent 1-D perturbation models for a fast fluidized bed considering compressibility effects. The first model is the explicit summation of incompressible and compressible terms. All compressible terms appear multiplied by the inverse squared gas sound propagation speed, s. *In the second model, a lumped waving structure is presented, with just one term corresponding to each wave hierarchy. In both proposed models, the incompressible part was retrieved in the limit* $s \rightarrow \infty$. *The Liu's linear stability analysis, based on Whitham's, was extended to estimate the compressibility contribution. Stability conditions on the propagation speeds and a criterion on the wave number were developed. This method was applied to two physical systems whose solid properties differ widely. It was shown that the effect of the fluid compressibility is at least as important as the effect of the solid compressibility modulus.* © 2011 American Institute of Chemical Engineers *AIChE J,* 57: 2965–2976, 2011
Keywords: fast fluidization, fluidized bed stability, pressure wave propagation, compressibility effect, wave hierarchy, sound speed

Introduction

Circulating fluidized beds (CFB) usually operate under the fast fluidization regime where solid particles are carried up by a fluid. In this regime, the terminal velocity of particles and clusters is surpassed by the up-flowing carrier fluid velocity and a continuous two-phase mixture flow takes place at the top exit. A convenient way to maintain long time operation is by solid recirculation which enhances the contact surface between phases and reduces interfacial heat and mass transfer resistances minimizing high changes in the state variables.

The pressure effect in CFB for several flow regimes was studied by Gidaspow[1] in 1994. Then, the measurement of the propagation speed of pressure waves in a CFB with the solid volume fraction dependent on the vertical position in the bed, was carried out by van der Schaaf et al.[2] They measured locally the pressure propagation speed at several solid volume fractions by placing a set of pressure transducers at several heights. Subsequently, De Wilde et al.[3] proposed a formula to estimate the mixture speed of sound. They also explored a filtering method by incorporating expressions for the added mass effect and the history term for a spherical particle, at the averaged level of description. However, their nonfiltered mixture speed of sound fitted better the van der Schaaf's et al.[2] experimental results than their filtered result.

Some studies on pressure waves in fluidized beds involve both the dense regime and the diluted regime. Bi et al.[4] studied the propagation velocity of pressure waves by the pseudo-homogeneous compressible wave theory and the separated flow compressible wave theory, for the groups of particles A and B,

Correspondence concerning this article should be addressed to A. Soria at asor@xanum.uam.mx.

finding insignificant differences in the results. Musmarra et al.[5] used a pseudo-homogeneous simplified expression for pressure waves obtained by Wallis[6] and a separated flow expression derived by Gregor and Rumpf.[7] Following Atkinson and Kytömaa,[8] they considered the propagation speed of pressure waves as a function of the frequency. From their results (for void fraction > 0.35), they found that the dynamic waves observed in their experiments are more elastic than compression waves.

Linear stability criteria for one-dimensional (1-D) incompressible two-phase flow models were obtained by Jones and Prosperetti,[9] by incorporating different effects such as surface tension, viscosity, correlation effects, and added mass. A different stability criterion for the incompressible model was proposed by Song and Ishii,[10] by relaying on the momentum flux parameters evaluation. Recently, Bi[11] found a significant dependence on the wave frequency for the propagation wave velocity in fluidized dense phase flows on Song and Ishii,[10] by using the pseudo-homogeneous pressure wave propagation expression of Gregor and Rumpf.[7]

The perturbation propagation velocities were obtained by Ryzhkov and Tolmachev[12] who also studied resonance in vibrating fluidized beds. Bi[11] reviewed their separated flows expression and reported a significant dependence on the wave frequency for the propagation wave velocity in fluidized dense phase flows. At present, acoustical methods are actively being researched due to their promise for cheap and effective methods for data acquisition in granular systems.[13]

Other works analyze compressible models[14–17] include Ransom and Hicks,[18] which discuss compressible 1-D, transient, two-pressure models for two-phase separated flows. These models give rise to a system of hyperbolic equations with greater physical meaning than single pressure models. Liu[19] studies the stability condition in fluidized beds following Whitham,[20] who shows that the relevant propagation speed of the higher order wave motion must be greater than the propagation speed of the lower order wave motion. Liu found that the stability condition is not satisfied when the higher order waves have wave speeds lower than the lower order waves.

In the present work, the incompressibility assumption is revisited. A methodology which allows the comparison between the incompressible and the compressible models is presented. For this purpose, in Section Wave Hierarchies the theoretical development used to obtain the incompressible and the compressible linearized perturbation models is established. Then in Section Stability Analysis, the Whitham stability analysis by phase velocity approximations and extensions to the approach by Liu in fluidized beds is performed. In Section Results and Discussion, this method is applied to an FCC powder catalyst dragged by water vapor at isothermal conditions and to the Sand-air system reported by van der Schaaf et al.[2] Finally, the main conclusions of this work are summarized.

Wave Hierarchies

Model equations

The physical system consists of a dispersion of rigid, spherical small particles of mean diameter d_p and intrinsic density ρ_s, moving within a gas or steam current in a vertical pipe at constant temperature. The fluid is considered to be a compressible Newtonian gas of intrinsic averaged density ρ_g and constant viscosity μ_g. The solid volume fraction ε_s, is set between 0 and 0.5 and satisfies $\varepsilon_g + \varepsilon_s = 1$, where ε_g is the gas volume fraction. The mixture is moving with an average mixture velocity $U_m = \varepsilon_s V_s + \varepsilon_g V_g$, where V_g and V_s are the gas and the solid up-flow mass-weighted mean velocities, respectively. The viscous effects are significant only close to the granule surfaces, since the mixture is considered to be highly turbulent. The particle Reynolds number is $Re_p = d_p \rho_g U_t/\mu_g$, where $U_t = |V_s - U_m| = \varepsilon_g (V_g - V_s)$ is the terminal velocity. In this model, viscosity effects in the bulk phases and turbulent stresses are neglected.

A space-time averaging method is applied to the local-instantaneous continuity and momentum equations for the gas and the solid phases. Therefore the following closed, nonlinear set of one-dimensional space-time averaged equations for the dependent variables $\{\varepsilon_g, p_g, V_g, V_s\}$ is obtained,[21–23]

$$\frac{\partial}{\partial t}\left[\varepsilon_g \rho_g(p_g)\right] + \frac{\partial}{\partial z}\left[\varepsilon_g \rho_g(p_g) V_g\right] = 0, \tag{1}$$

$$-\rho_s \frac{\partial}{\partial t}\varepsilon_g + \rho_s \frac{\partial}{\partial z}\left[(1-\varepsilon_g) V_s\right] = 0, \tag{2}$$

$$\frac{\partial}{\partial t}\left[\varepsilon_g \rho_g(p_g) V_g\right] + \frac{\partial}{\partial z}\left[\varepsilon_g \rho_g(p_g) V_g^2\right] + \varepsilon_g \frac{\partial}{\partial z} p_g + F + \rho_g(p_g) g = 0, \tag{3}$$

$$\rho_s \frac{\partial}{\partial t}\left[(1-\varepsilon_g) V_s\right] + \rho_s \frac{\partial}{\partial z}\left[(1-\varepsilon_g) V_s^2\right] + (1-\varepsilon_g)\frac{\partial}{\partial z} p_g - \Phi'(1-\varepsilon_g)\frac{\partial}{\partial z}\varepsilon_g - F + (1-\varepsilon_g)\left[\rho_s - \rho_g(p_g)\right] g = 0. \tag{4}$$

Here z and t are the vertical coordinate and the time, respectively, g is the gravitational force per unit mass and p_g is the averaged gas phase pressure; the solid grains density $\rho_s = \rho_{s0}$, is a constant. The averaged solid phase pressure p_s is modeled through the closure $p_s = p_g + \Phi(\varepsilon_s)$ in Eq. 4, where the function $\Phi(\varepsilon_s)$ is the solid compressibility modulus and $\Phi' = d\Phi/d\varepsilon_s$. The simpler closure $p_s = \Phi(\varepsilon_s)$ reduces the coupling of the momentum balances to the interaction force F between fluid and particles. This closure was used by Jackson[24] and Liu[19] among others and it was recommended by Gidaspow.[1]

On the other hand, Jackson[24] considered two contributions to F: a dominant drag force and a virtual mass effect. Only the former contribution is considered here, so that $F = \beta \varepsilon_g (1 - \varepsilon_g)(V_g - V_s)$, where $\beta = (3/4 d_p) C_D \rho_g U_t$ is an interaction parameter. Also, Jackson,[24] Liu,[19] and Homsy et al.[25] considered an effective viscosity effect in the dense fluidization regime, which is not taken into account here. The main difference between the present work and Refs. 19, 24, and 25, is the structure of equations obtained which shows explicitly the compressibility effect over the incompressibility effect. Besides, the compressibility was introduced through an explicit state equation of the gas phase in a fast fluidization regime.

To obtain perturbation wave hierarchies for both the incompressible and the compressible models, waving solutions for linearized Eq. 1 to Eq. 4 are proposed. The linearization is carried out around a uniform base state (denoted by a zero sub-index) plus small perturbations such that $\varepsilon_g = \varepsilon_0 + \varepsilon$, $p_g = p_0 + p$, $V_g = v_{g0} + v_g$, and $V_s = v_{s0} + v_s$. In the next subsection, the linearized equations are represented in matrix form and later on the comparative coefficients analysis between the models is presented.

Statement of the problem

Let

$$\mathbf{u} = (\,\varepsilon \quad p \quad v_g \quad v_s\,)^T \tag{5}$$

be the perturbation vector for the linearized partial differential equation (PDE) first-order system,

$$\mathbf{B}\frac{\partial \mathbf{u}}{\partial t} + \mathbf{C}\frac{\partial \mathbf{u}}{\partial z} + \mathbf{D}\mathbf{u} = \mathbf{0}, \tag{6}$$

where the matrices **B**, **C,** and **D** are the linearized coefficients of Eq. 1 to Eq. 4, given in Appendix A. The spatial derivatives of the velocity fluctuations v_g and v_s can be obtained from the continuity equations, then they are substituted into the momentum equations to arrive to two second-order linearized equations for void fraction (ε) and pressure (p) fluctuations, namely,

$$L_1\varepsilon + \left[L_3 + \left(\frac{d\rho_g}{dp_g}\right)_0 K_1\right]p = 0, \tag{7}$$

$$L_2\varepsilon + \left[L_3 + \left(\frac{d\rho_g}{dp_g}\right)_0 K_2\right]p = 0. \tag{8}$$

The second-order differential operators L_1, L_2, L_3, and K_1, as well as the first-order operator K_2, are given by

$$L_1 = -\frac{\rho_{g0}}{\varepsilon_0}\left(\frac{\partial}{\partial t} + v_{g0}\frac{\partial}{\partial z}\right)^2 - \beta\left(\frac{\partial}{\partial t} + v_{g0}\frac{\partial}{\partial z}\right) - \frac{1-\varepsilon_0}{\varepsilon_0}\beta\left(\frac{\partial}{\partial t} + v_{s0}\frac{\partial}{\partial z}\right), \tag{9}$$

$$L_2 = \frac{\rho_{s0}}{1-\varepsilon_0}\left(\frac{\partial}{\partial t} + v_{s0}\frac{\partial}{\partial z}\right)^2 + \frac{\varepsilon_0}{1-\varepsilon_0}\beta\left(\frac{\partial}{\partial t} + v_{g0}\frac{\partial}{\partial z}\right) + \beta\left(\frac{\partial}{\partial t} + v_{s0}\frac{\partial}{\partial z}\right) - \Phi_0'\frac{\partial^2}{\partial z^2} - \frac{(\rho_{s0}-\rho_{g0})}{1-\varepsilon_0}g\frac{\partial}{\partial z}, \tag{10}$$

$$L_3 = \frac{\partial^2}{\partial z^2}, \tag{11}$$

$$K_1 = -\left(\frac{\partial}{\partial t} + v_{g0}\frac{\partial}{\partial z}\right)^2 - (1-\varepsilon_0)\frac{\beta}{\rho_{g0}}\left(\frac{\partial}{\partial t} + v_{g0}\frac{\partial}{\partial z}\right) + \frac{g}{\varepsilon_0}\frac{\partial}{\partial z}, \tag{12}$$

$$K_2 = \varepsilon_0\frac{\beta}{\rho_{g0}}\left(\frac{\partial}{\partial t} + v_{g0}\frac{\partial}{\partial z}\right) - g\frac{\partial}{\partial z}. \tag{13}$$

The factor $(d\rho_g/dp_g)_0$ accounts for the fluid density change as a function of the fluid pressure, through an isothermic state equation $\rho_g = \rho_g(p_g)$. The sound speed in a homogeneous gas can now be introduced by considering the relationship $(d\rho_g/dp_g)_0 = s^{-2}$, where s is the sound speed in a pure gas. The incompressible fluid approximation can be retrieved from Eq. 7 and Eq. 8 by taking the limit $(d\rho_g/dp_g)_0 = 0$ or, equivalently when $s \to \infty$. Under the incompressibility approximation, a second-order PDE for ε can be found by direct subtraction of Eq. 7 from Eq. 8, yielding $(L_2 - L_1)\varepsilon = 0$. Also, a fourth-order PDE for p can be alternatively obtained by cross application of L_2 and L_1 operators onto Eqs. 7 and 8, respectively, and further subtraction to get $(L_2 - L_1)L_3\, p = 0$. Thus, while void fraction dynamics is represented by a second-order PDE, pressure fluctuation dynamics is the same PD operator applied onto a second-order spatial derivative. Moreover, if a solid pressure closure, such as $p_s = \Phi(\varepsilon_s)$ is used, decoupling of the pressure term is allowed since the solid momentum balance gives the reduced form $L_2\,\varepsilon = 0$. The whole compressible behavior can also be expressed as a wave equation for ε or for p. Thus, cross application of L_2 and L_1 operators onto Eqs. 7 and 8 and further subtraction gives a fourth-order PDE for pressure perturbations. An alternative procedure gives the same PDE for volume fraction perturbations, that is

$$\left[(L_2 - L_1)L_3 - \frac{1}{s^2}(L_1K_2 - L_2K_1)\right]\varphi = 0, \tag{14}$$

where φ is either ε or p. The incompressible wave behavior of ε perturbations is represented by the differential operator $(L_2 - L_1)$, which can be decomposed and analyzed in a similar way as done by Liu[19] for a fluidized bed, incorporating the differences in the fluidization regime and in the physical effects accounted for. In this way, we get

$$L_2 - L_1 = \frac{\rho_{g0}}{\varepsilon_0}\left(\frac{\partial}{\partial t} + v_{g0}\frac{\partial}{\partial z}\right)^2 + \frac{\rho_{s0}}{1-\varepsilon_0}\left(\frac{\partial}{\partial t} + v_{s0}\frac{\partial}{\partial z}\right)^2 + \frac{\beta}{1-\varepsilon_0}\left(\frac{\partial}{\partial t} + v_{g0}\frac{\partial}{\partial z}\right) + \frac{\beta}{\varepsilon_0}\left(\frac{\partial}{\partial t} + v_{s0}\frac{\partial}{\partial z}\right) - \Phi_0'\frac{\partial^2}{\partial z^2} - \frac{(\rho_{s0}-\rho_{g0})}{1-\varepsilon_0}g\frac{\partial}{\partial z}, \tag{15}$$

where the second-order wave terms represent the fluid and particle inertial effects, while the first-order wave terms come from the interfacial drag force fluctuations. The second-order and the first-order spatial terms are related, respectively, to the solid phase compressibility modulus and the buoyancy force fluctuations. The differential operator $(L_2 - L_1)$ is further modified by $L_3 p$, a second-order spatial operator applied to p. This can be visualized as a dispersion effect on the second-order waving structure. Also, this term gives raise to fourth- and third-order differential terms governing the pressure fluctuation dynamics under the incompressibility approximation. On the other hand, the operator $(L_2K_1 - L_1K_2)$ is the dynamic contribution of the fluid density onto all the above mentioned forces, giving their correspondent interaction effects. This operator is weighted by the s^{-2} factor and is given by

$$\begin{aligned}
-(L_2K_1 - L_1K_2) = {} & \left[-\frac{\rho_{s0}}{1-\varepsilon_0}\left(\frac{\partial}{\partial t} + v_{s0}\frac{\partial}{\partial z}\right)^2 + \Phi_0'\frac{\partial^2}{\partial z^2}\right] \\
& \times \left(\frac{\partial}{\partial t} + v_{g0}\frac{\partial}{\partial z}\right)^2 + \left[\frac{1-2\varepsilon_0}{1-\varepsilon_0}\beta\left(\frac{\partial}{\partial t} + v_{g0}\frac{\partial}{\partial z}\right) - \beta\left(\frac{\partial}{\partial t} + v_{s0}\frac{\partial}{\partial z}\right) \right. \\
& \left. + \frac{\varepsilon_0\rho_{s0} - \rho_{g0}}{\varepsilon_0(1-\varepsilon_0)}g\frac{\partial}{\partial z}\right]\left(\frac{\partial}{\partial t} + v_{g0}\frac{\partial}{\partial z}\right)^2 + \left[-\beta\frac{\rho_{s0}}{\rho_{g0}}\left(\frac{\partial}{\partial t} + v_{g0}\frac{\partial}{\partial z}\right) \right. \\
& \left. + \frac{\rho_{s0}g}{\varepsilon_0(1-\varepsilon_0)}\frac{\partial}{\partial z}\right]\left(\frac{\partial}{\partial t} + v_{s0}\frac{\partial}{\partial z}\right)^2 + (1-\varepsilon_0)\Phi_0'\frac{\beta}{\rho_{g0}} \\
& \times \left(\frac{\partial}{\partial t} + v_{g0}\frac{\partial}{\partial z}\right)\frac{\partial^2}{\partial z^2} - \frac{1}{\varepsilon_0}\Phi_0'g\frac{\partial^3}{\partial z^3} + \left(\frac{\rho_{s0}}{\rho_{g0}} - \frac{1-2\varepsilon_0}{1-\varepsilon_0}\right) \\
& \times \beta g\left(\frac{\partial}{\partial t} + v_{g0}\frac{\partial}{\partial z}\right)\frac{\partial}{\partial z} + \beta g\left(\frac{\partial}{\partial t} + v_{s0}\frac{\partial}{\partial z}\right)\frac{\partial}{\partial z} \\
& - \frac{\rho_{s0} - \rho_{g0}}{\varepsilon_0(1-\varepsilon_0)}g^2\frac{\partial^2}{\partial z^2}.
\end{aligned} \tag{16}$$

In Eq. 16 both, waving and dispersive interactions are accounted for, as well as spatial interactions. These are associated to fluid and solid inertial forces, solid compressibility, viscous interfacial drag and buoyancy. None of these

forces appears by itself in Eq. 16, but as pair interactions with other effects. Each one of these pairs represents the enhancement due to the couple of forces considered, due to the fluid density change. The point here is to quantify the magnitude of such enhancement when compared with the incompressible model.

Waving structures

By substituting the differential operators given by Eqs. 15 and 16 into Eq. 14 and casting them into a lumped waving structure, the following equivalent differential form is obtained

$$(L_2 - L_1)L_3 - \frac{1}{s^2}(L_1K_2 - L_2K_1) = \left[\tau\left(\frac{\partial}{\partial t} + c_1\frac{\partial}{\partial z}\right)\left(\frac{\partial}{\partial t} + c_2\frac{\partial}{\partial z}\right) + \left(\frac{\partial}{\partial t} + a\frac{\partial}{\partial z}\right)\right]\frac{\partial^2}{\partial z^2} - \frac{1}{s^2}\begin{bmatrix} T\left(\frac{\partial}{\partial t}+\eta_{41}\frac{\partial}{\partial z}\right)\left(\frac{\partial}{\partial t}+\eta_{42}\frac{\partial}{\partial z}\right)\left(\frac{\partial}{\partial t}+\eta_{43}\frac{\partial}{\partial z}\right)\left(\frac{\partial}{\partial t}+\eta_{44}\frac{\partial}{\partial z}\right) \\ +C\left(\frac{\partial}{\partial t}+\eta_{31}\frac{\partial}{\partial z}\right)\left(\frac{\partial}{\partial t}+\eta_{32}\frac{\partial}{\partial z}\right)\left(\frac{\partial}{\partial t}+\eta_{33}\frac{\partial}{\partial z}\right) \\ -gC\left(\frac{\partial}{\partial t}+\eta_{21}\frac{\partial}{\partial z}\right)\frac{\partial}{\partial z} \end{bmatrix}. \quad (17)$$

Here we have used the notation favored by Liu,[19] to denote the parameters corresponding to the basic incompressible behavior. The relaxation times τ and T are

$$\tau = \frac{(1-\varepsilon_0)\rho_{g0} + \varepsilon_0\rho_{s0}}{\beta}, \quad (18)$$

$$T = \frac{\varepsilon_0\rho_{s0}}{\beta}, \quad (19)$$

and the dimensionless coefficient C is defined as

$$C = \varepsilon_0\frac{\varepsilon_0\rho_{g0} + (1-\varepsilon_0)\rho_{s0}}{\rho_{g0}}. \quad (20)$$

The propagation speeds were found by solving different sets of algebraic equations for incompressible and compressible cases, as will be discussed below. The incompressible second-order propagation speeds c_1 and c_2 were found as the solutions of Eqs. B.01 and B.02, in Appendix B, yielding

$$c_1, c_2 = \frac{(1-\varepsilon_0)\rho_{g0}v_{g0} + \varepsilon_0\rho_{s0}v_{s0}}{(1-\varepsilon_0)\rho_{g0} + \varepsilon_0\rho_{s0}} \pm \frac{\sqrt{\varepsilon_0(1-\varepsilon_0)\rho_{g0}\rho_{s0}\left[\left(\frac{1-\varepsilon_0}{\rho_{s0}} + \frac{\varepsilon_0}{\rho_{g0}}\right)\Phi_0' - \left(v_{g0} - v_{s0}\right)^2\right]}}{(1-\varepsilon_0)\rho_{g0} + \varepsilon_0\rho_{s0}}. \quad (21)$$

The propagation speeds for the compressible model were obtained from sets of algebraic equations made up by fitting polynomials expanded from Eq. 17 and those in original variables, Eqs. 15 and 16 (See Appendix B). The expressions for a and η_{21} were found to be

$$a = \varepsilon_0 v_{g0} + (1-\varepsilon_0)v_{s0} - \varepsilon_0\left(\rho_{s0} - \rho_{g0}\right)\frac{g}{\beta}, \quad (22)$$

$$\eta_{21} = \frac{(2\varepsilon_0 - 1)\rho_{g0}v_{g0} + (1-\varepsilon_0)\rho_{s0}v_{g0} + (1-\varepsilon_0)\rho_{g0}v_{s0} + \rho_{g0}\left(\rho_{s0} - \rho_{g0}\right)\frac{g}{\varepsilon_0\beta}}{\varepsilon_0\rho_{g0} + (1-\varepsilon_0)\rho_{s0}}. \quad (23)$$

Similar procedure for the compressible fourth-order propagation speeds η_{4k}, $k = 1,2,3,4$ gives

$$\eta_{41} = \eta_{42} = v_{g0}, \quad (24a)$$

$$\eta_{43}, \eta_{44} = v_{s0} \pm \sqrt{\frac{1-\varepsilon_0}{\rho_{s0}}\Phi_0'}. \quad (24b)$$

These roots are real and coincident with the eigenvalues of the characteristic polynomial of the linearized PDE first-order system, Eq. 6. Therefore the system is stable in the sense of being hyperbolic, but not totally hyperbolic since $\eta_{41} = \eta_{42}$.

Expressions of the third-order propagation speeds η_{31}, η_{32}, and η_{33} were found from Eqs. B.10 to B.12. Since the whole expressions in primitive parameters are too length and complex to be included explicitly, we present numerical computations.

To simplify Eq. 17 further, we consider its dimensionless form which is obtained by using the column length L and the arithmetic mean velocity $U_0 = (V_{g0} + V_{s0})/2$ as scaling parameters. The dimensionless variables are $z' = z/L$, $a' = a/U_0$, $t' = tU_0/L$ and all the dimensionless propagation speeds can be defined in a way similar to a'. Therefore, from Eq. 17 we may be able to get

$$\left[\tau'\left(\frac{\partial}{\partial t'}+c_1'\frac{\partial}{\partial z'}\right)\left(\frac{\partial}{\partial t'}+c_2'\frac{\partial}{\partial z'}\right)\frac{\partial^2}{\partial z'^2} + \left(\frac{\partial}{\partial t'}+a'\frac{\partial}{\partial z'}\right)\frac{\partial^2}{\partial z'^2}\right]\varphi - C'\begin{bmatrix} T'\left(\frac{\partial}{\partial t'}+\eta_{41}'\frac{\partial}{\partial z'}\right)\left(\frac{\partial}{\partial t'}+\eta_{42}'\frac{\partial}{\partial z'}\right)\left(\frac{\partial}{\partial t'}+\eta_{43}'\frac{\partial}{\partial z'}\right) \\ \left(\frac{\partial}{\partial t'}+\eta_{44}'\frac{\partial}{\partial z'}\right) \\ +\left(\frac{\partial}{\partial t'}+\eta_{31}'\frac{\partial}{\partial z'}\right)\left(\frac{\partial}{\partial t'}+\eta_{32}'\frac{\partial}{\partial z'}\right)\left(\frac{\partial}{\partial t'}+\eta_{33}'\frac{\partial}{\partial z'}\right) \\ -G'\left(\frac{\partial}{\partial t'}+\eta_{21}'\frac{\partial}{\partial z'}\right)\frac{\partial}{\partial z'} \end{bmatrix}\varphi = 0, \quad (25)$$

where prime indexes denote dimensionless coefficients, $\tau' = U_0\tau/L$, $T' = U_0T/LC$, $C' = (U_0/s)^2\,C$, and $G' = Lg/U_0^2$. It should be pointed out that the compressible fourth-order wave can be neglected, when compared with the third order one, if $T' \ll 1$. Since $\rho_{s0} \gg \rho_{g0}$ this condition is fulfilled if $\tau' << \frac{\rho_{s0}}{\rho_{g0}}(1-\varepsilon_0)\varepsilon_0$, which is readily satisfied, but in a narrow zone close to the limit when $\varepsilon_0 \to 1$. Outside this zone, where

$$\varepsilon_{s0} > \varepsilon_{s0,\min} \approx \frac{1}{2} - \sqrt{\frac{1}{4} - 100\frac{\rho_{g0}}{\rho_{s0}}\tau'}, \quad (26)$$

the compressibility effect associated to fourth-order terms is negligible as compared to third-order and second-order compressible terms. Thus, a simplified model from Eq. 17 is

$$\left[\tau\left(\frac{\partial}{\partial t} + c_1\frac{\partial}{\partial z}\right)\left(\frac{\partial}{\partial t} + c_2\frac{\partial}{\partial z}\right) + \left(\frac{\partial}{\partial t} + a\frac{\partial}{\partial z}\right)\right]\frac{\partial^2}{\partial z^2}\varphi - \frac{C}{s^2}\left[\left(\frac{\partial}{\partial t}+\eta_{31}\frac{\partial}{\partial z}\right)\left(\frac{\partial}{\partial t}+\eta_{32}\frac{\partial}{\partial z}\right)\left(\frac{\partial}{\partial t}+\eta_{33}\frac{\partial}{\partial z}\right) - g\left(\frac{\partial}{\partial t}+\eta_{21}\frac{\partial}{\partial z}\right)\frac{\partial}{\partial z}\right]a = 0, \quad (27)$$

or combining third-order terms:

$$\tau\left(\frac{\partial}{\partial t}+c_1\frac{\partial}{\partial z}\right)\left(\frac{\partial}{\partial t}+c_2\frac{\partial}{\partial z}\right)\frac{\partial^2}{\partial z^2}\varphi - \frac{C}{s^2}\left[\left(\frac{\partial}{\partial t}+\alpha_1\frac{\partial}{\partial z}\right)\left(\frac{\partial}{\partial t}+\alpha_2\frac{\partial}{\partial z}\right)\left(\frac{\partial}{\partial t}+\alpha_3\frac{\partial}{\partial z}\right) -g\left(\frac{\partial}{\partial t}+\eta_{21}\frac{\partial}{\partial z}\right)\frac{\partial}{\partial z}\right]\varphi=0. \quad (27b)$$

Here α_i, $i = 1,2,3$ are the propagation speeds that account for both the compressible and the incompressible behavior and are the roots of the polynomial equation

$$\alpha^3 - P_1\alpha^2 + \left(P_2 - \frac{s^2}{C}\right)\alpha - \left(P_3 - \frac{s^2 a}{C}\right) = 0 \quad (28)$$

where the polynomials P_k, $k = 1,2,3$ are given in Appendix B. Although Eqs. 27a and 27b are equivalent, different aspects that correspond to the physical behavior of each one can be observed. In the first square bracket of Eq. 27a, the original structure of the incompressible model, when compared with Liu[19] is apparent. Nevertheless, the first and second-order waves in this bracket are applied onto a second-order spatial derivative. On the other hand, a lumped waving structure is presented in Eq. 27b with just one term corresponding to each wave hierarchy. In Eq. 27a, the compressibility effect is wholly expressed in the second square bracket term with a coefficient proportional to s^{-2}, leading to the incompressible model as $s \to \infty$ and with propagation speeds, η_{ij}, independent of the sound speed s. By contrast, in Eq. 27b the propagation speeds α_1 and α_3 are highly dependent on s, and the process to get the incompressible model by making $s \to \infty$, should take care of the limiting values of these propagation speeds $\alpha_j \to \pm\infty, j = 1,3$. This can be obtained when the product of hyperbolic operators gives raise to the parabolic behavior expressed by the $\partial^2/\partial z^2$ operator, together with the fact that $\alpha_2 \to a$. Furthermore, the compressible second-order term, in either Eq. 27a or Eq. 27b, is a degenerated second-order wave associated to gravity effects with just one finite propagation speed.

Stability Analysis

Whitham stability analysis by phase velocity approximations

To obtain stability criteria, it is assumed that solutions for $\varphi(z,t)$ in Eq. 27b are given by the wave functions[20] $\varphi(z,t) = Ae^{i(\kappa z - \omega t)}$, where $\kappa \in \mathbb{R}$ is the (real) wave number and $\omega = \omega_R + i\omega_I \in \mathbb{C}$ is the (complex) attenuation wave factor. Therefore, it must be satisfied that $\omega_1 < 0$ to obtain a stability condition. Application of this solution to Eq. 27b yields

$$\tau(c_1\kappa-\omega)(c_2\kappa-\omega)\kappa^2 - \frac{C}{s^2}\left[\begin{array}{c} -i(\alpha_1\kappa-\omega)(\alpha_2\kappa-\omega)(\alpha_3\kappa-\omega) \\ +g(\eta_{21}\kappa-\omega)\kappa \end{array}\right] = 0. \quad (29)$$

Now, it is possible to analyze the wave speed behavior close to each one of the phase velocities, following the Whitham[20] criterion on wave hierarchies. To work out some inequalities that will be used later on, let us assume that the relative size of the propagation speeds are such that $c_1 > c_2$ and $\alpha_1 > \alpha_2 > \alpha_3$. Therefore, considering a phase velocity close to α_1, we propose to analyze Eq. 29 under a waving action $\omega \to \alpha_1\,\kappa$ such that

$$\tau(c_1-\alpha_1)(c_2-\alpha_1)\kappa^2 + i\frac{C}{s^2}(\alpha_1\kappa-\omega)(\alpha_2-\alpha_1)(\alpha_3-\alpha_1) - \frac{Cg}{s^2}(\eta_{21}-\alpha_1) = 0. \quad (30)$$

This implies that

$$\omega = \alpha_1\kappa + i\frac{Cg(\eta_{21}-\alpha_1) - s^2\kappa^2\tau(c_1-\alpha_1)(c_2-\alpha_1)}{C(\alpha_2-\alpha_1)(\alpha_3-\alpha_1)}, \quad (31)$$

where its imaginary part should satisfy the inequality

$$\omega_I = \frac{Cg(\eta_{21}-\alpha_1) - s^2\kappa^2\tau(c_1-\alpha_1)(c_2-\alpha_1)}{C(\alpha_2-\alpha_1)(\alpha_3-\alpha_1)} < 0, \quad (32)$$

to be stable. Considering the assumptions $c_1 > c_2$ and $\alpha_1 > \alpha_2 > \alpha_3$, given above, Eq. 32 can be simplified to the condition

$$-(\alpha_1-c_1)(\alpha_1-c_2) < -\frac{Cg}{\tau s^2\kappa^2}(\eta_{21}-\alpha_1). \quad (33)$$

A similar procedure for $\omega \to \alpha_2\,\kappa$, $\omega \to \alpha_3\,\kappa$, $\omega \to \eta_{21}\,\kappa$, $\omega \to c_1\,\kappa$, and $\omega \to c_2\,\kappa$, gives

$$(\alpha_2-c_1)(\alpha_2-c_2) < \frac{Cg}{\tau s^2\kappa^2}(\eta_{21}-\alpha_2), \quad (34)$$

$$-(\alpha_3-c_1)(\alpha_3-c_2) < -\frac{Cg}{\tau s^2\kappa^2}(\eta_{21}-\alpha_3), \quad (35)$$

$$(\eta_{21}-\alpha_1)(\eta_{21}-\alpha_2)(\eta_{21}-\alpha_3) < 0, \quad (36)$$

$$-(\alpha_1-c_1)(\alpha_2-c_1)(\alpha_3-c_1) < 0 \quad (37)$$

and

$$(\alpha_1-c_2)(\alpha_2-c_2)(\alpha_3-c_2) < 0, \quad (38)$$

respectively. Since $\alpha_1 > \alpha_2 > \alpha_3$ inequality (36) implies that η_{21} must be such that $\alpha_1 > \eta_{21} > \alpha_2$ or $\alpha_3 > \eta_{21}$. Similarly, inequality (37) requires that c_1 must be such that $\alpha_1 > c_1 > \alpha_2$ or $\alpha_3 > c_1$, and inequality (38) that c_2 must be such that $\alpha_2 > c_2 > \alpha_3$. Therefore, we find that both sequences $\alpha_1 > c_1 > \alpha_2 > c_2 > \alpha_3$ and $\alpha_1 > \eta_{21} > \alpha_2$ should be satisfied or $\alpha_1 > c_1 > \alpha_2 > c_2 > \alpha_3 > \eta_{21}$ for the system to be stable. In Section Results and Discussion, it will be found by numerical computations that η_{21} is not the smallest propagation speed, therefore the later inequality will not be processed further. If we have $\alpha_1 > c_1 > \alpha_2 > c_2 > \alpha_3$ and $\alpha_1 > \eta_{21} > \alpha_2$, inequalities (33) to (35) give rise to

$$\frac{(\alpha_1-c_1)(\alpha_1-c_2)}{(c_1-\alpha_3)(c_2-\alpha_3)} > -\frac{(\alpha_1-\eta_{21})}{(\eta_{21}-\alpha_3)}, \quad (39)$$

$$\frac{(c_1-\alpha_2)(\alpha_2-c_2)}{(c_1-\alpha_3)(c_2-\alpha_3)} > -\frac{(\eta_{21}-\alpha_2)}{(\eta_{21}-\alpha_3)}, \quad (40)$$

and

$$\frac{\tau s^2\kappa^2}{Cg}(c_2-\alpha_3) > \frac{(\eta_{21}-\alpha_3)}{(c_1-\alpha_3)}, \quad (41)$$

Table 1. Parameter Values and Operating Conditions at Ground States

Parameter	FCC Catalyst-Vapor	Sand-Air
Sound speed in pure fluid, s (m/s)	655	346
Solid density, ρ_{s0} (kg/m^3)	1300	2650
Fluid density, ρ_{g0} (kg/m^3)	0.7065	0.9340
Solid grain diameter, d_p (μm)	60	310
Terminal velocity, U_t (m/s)	0.085	2.231
Superficial fluid velocity, U_g (m/s)	7.000	3.200
Column diameter, D_t (m)	1.168	0.960
Column length, L (m)	22	9
Fluid Reynolds number, Re_g	1.93×10^5	1.43×10^5
Solid Reynolds number, Re_s	0.12	32.30
Stokes number, St	0.13	2.15

as other forms of the same stability conditions. Since all terms in Eqs. 39 and 40 are positive, it follows that there are no additional restrictions arising from these conditions. Moreover, Eq. 41 can be recast as a limiting condition on the wave number:

$$\kappa > \kappa_0 = \sqrt{\frac{Cg}{\tau s^2}\frac{(\eta_{21}-\alpha_3)}{(c_1-\alpha_3)(c_2-\alpha_3)}}, \tag{42}$$

for the fluidized bed to be linearly stable.

Extensions to the approach by Liu

The previous analysis shows that gas compressibility increases the stability region as compared to the incompressible behavior. Alternatively, to develop a stability analysis following the approach by Liu,[19] we begin by the Fourier transforming Eq. 27a

$$[\tau(c_1\kappa-\omega)(c_2\kappa-\omega)-i(a\kappa-\omega)]\kappa^2 - \frac{C}{s^2}\begin{bmatrix} -i(\eta_{31}\kappa-\omega)(\eta_{32}\kappa-\omega)(\eta_{33}\kappa-\omega) \\ +g(\eta_{21}\kappa-\omega)\kappa \end{bmatrix} = 0. \tag{43}$$

In this equation, stability conditions can be found by consideration of waves moving close to the incompressible second-order velocities and then taking the limits $\omega \to c_1\,\kappa$ and $\omega \to c_2\,\kappa$. From Eq. 43, it follows that

$$c_1 + h_1 = c_1 - \frac{C}{s^2}\left(c_1^3 - P_1c_1^2 + P_2c_1 - P_3\right) > a > c_2 - \frac{C}{s^2}\left(c_2^3 - P_1c_2^2 + P_2c_2 - P_3\right) = c_2 - h_2, \tag{44}$$

where P_k, $k = 1,2,3$ are given in Appendix B. This criterion reduces to the well-known condition $c_1 > a > c_2$ in the incompressibility limit and clarifies how the compressibility effects modify these stability limits through the functions h_1 and h_2.

Results and Discussion

The procedure developed in Sections Wave Hierarchies and Stability Analysis was applied to two physical systems. The first one, a FCC catalyst carried up by a turbulent water vapor flow under physical similar conditions to those of a typical industrial riser unit.[26] The second one, a CFB Sand-air experimental system, as reported by van der Schaaf et al.[2]

Parameter values and operation conditions for an FCC catalyst-vapor system and a Sand-air system

In Table 1 we give the solid and fluid physical properties, as well as the relevant geometrical parameters and operation conditions in a homogeneous ground state for each system.

Notice that the FCC powder flow is governed by the gas drag to a larger extent than the Sand grain motion, as indicated by their Stokes number values. Also, their terminal velocities are quite different due to the disparity between the fluid and the solid flow velocities, which is much smaller for the FCC than for the sand. Moreover, it is assumed that the solids are delayed with respect to the mixture mean velocity, in an amount that corresponds to the terminal velocity. According to this assumption, the ground state solid volume fraction is given by

$$\varepsilon_{s0} = \frac{U_s}{U_m - U_t}. \tag{45}$$

To perform computations, either the superficial solid velocity U_s or the solid volume fraction, is assumed to be given. The solid-fluid interaction parameter β should be selected according to the solid Reynolds number value. This selection is done considering that the FCC grains are in the Stokes regime, while the sand grains are better described by a drag coefficient according to the Ergun's equation. The solid compressibility modulus, as given by Jiradilok et al.[27] $\varepsilon_{s0}\Phi_0' = 10^{6.837-2.475\varepsilon_0}$ was computed. In what follows both examples are examined together to appreciate their similarities and differences.

Comparison of wave coefficients and significance of wave hierarchies

Dimensionless coefficients of Eq. 25 are denoted by prime indexes, so that $\tau' = U_0\,\tau/L$, $T' = U_0T/LC$, $C' = (U_0/s)^2\,C$, and $G' = Lg/U_0^2$. Comparing these coefficients with respect

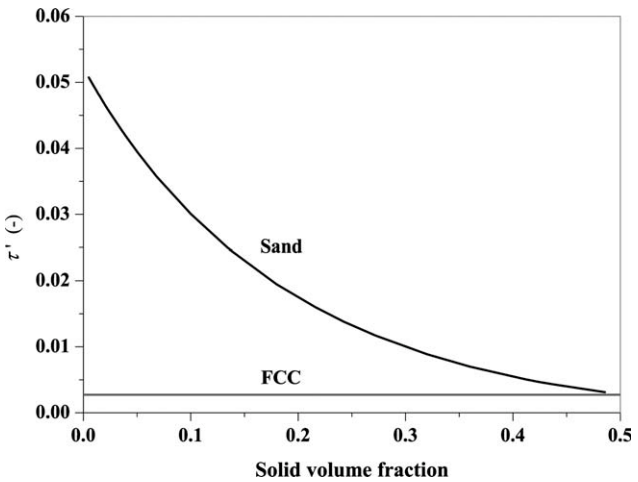

Figure 1. Dimensionless relaxation time τ' of the incompressible second-order differential operator for FCC (gray line) and Sand (black line).

Table 2. Limiting Values of the Solid Volume Fractions

System	$\varepsilon_{s0,\min}$	$\varepsilon_{s0,IC}$
FCC catalyst-vapor	0.0002	0.0125
Sand-air	0.0050	0.1680

to unity, the incompressible first-order wave coefficient gives an idea of the importance of each one of them as the solid volume fraction changes. Thus, in Figure 1 the incompressible second-order wave relaxation time can be appreciated. It should be remarked that for FCC τ' is close to a constant value around 0.0027. On the other hand, for the Sand system τ' is a decaying function with an initial value of 0.0507, which is 18 times greater than the FCC value. If T' is chosen such that $T' < 0.01$, the fourth-order wave coefficient can be neglected when compared with the compressible third-order wave coefficient of 1. This is satisfied for $\varepsilon_{s0} < \varepsilon_{s0,\min}$ according to Eq. 26 and values of $\varepsilon_{s0,\min}$ are given in Table 2 for the FCC and the Sand systems.

In Figure 2, τ' and C' are plotted as functions of ε_{s0}. A crossover between both plots is apparent at a given value $\varepsilon_{s0,IC}$, where $\tau' = C'$. Thus, for $\varepsilon_{s0} < \varepsilon_{s0,IC}$, the incompressible higher order term, governed by the solid compressibility modulus effect, is greater than the fluid compressibility

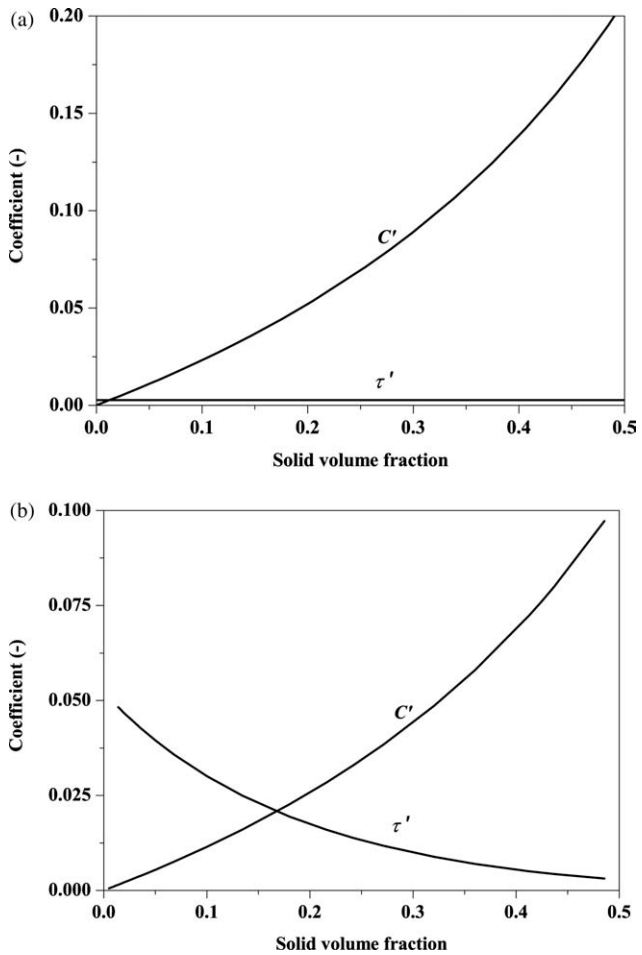

Figure 2. Dimensionless τ' and C' coefficients for a) FCC powder and b) Sand systems.

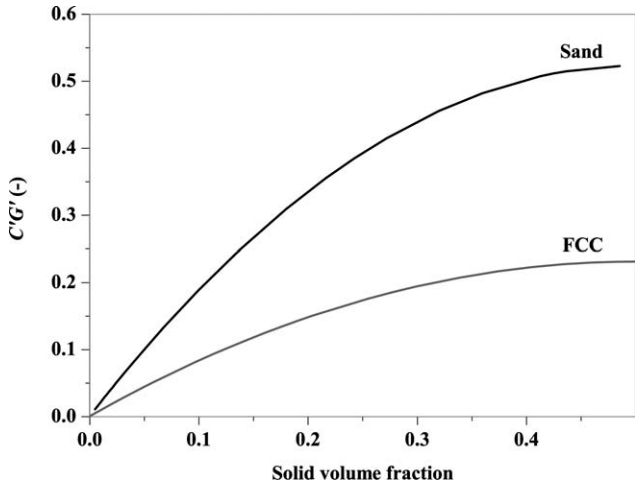

Figure 3. Dimensionless coefficients of the compressible (degenerate) second-order wave for FCC (gray line) and Sand (black line).

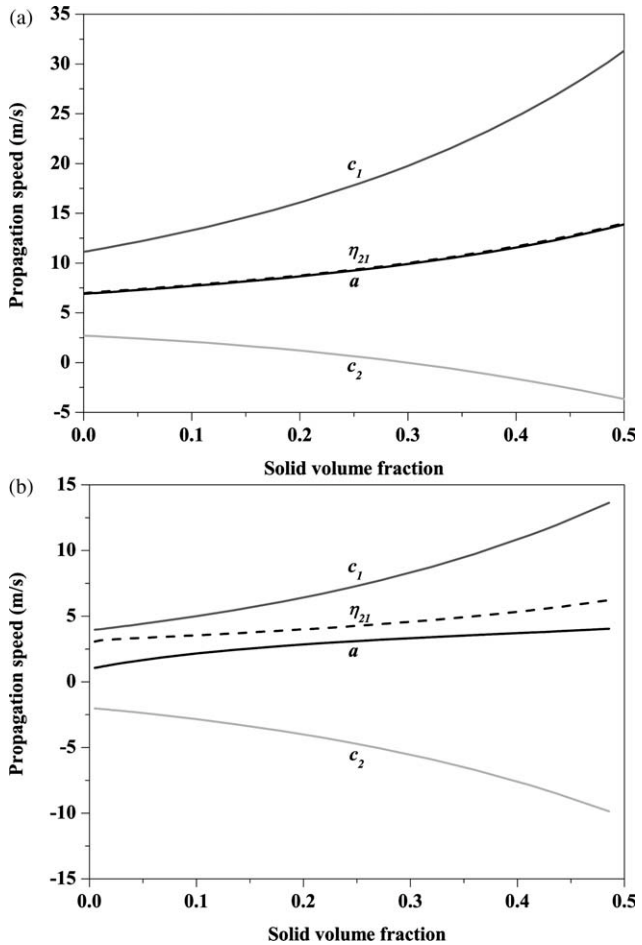

Figure 4. Incompressible first-order propagation speed a (black line), incompressible second-order propagation speeds c_1 and c_2 (gray lines) and compressible incomplete second-order speed η_{21} (dashed line), for (a) FCC and (b) Sand systems.

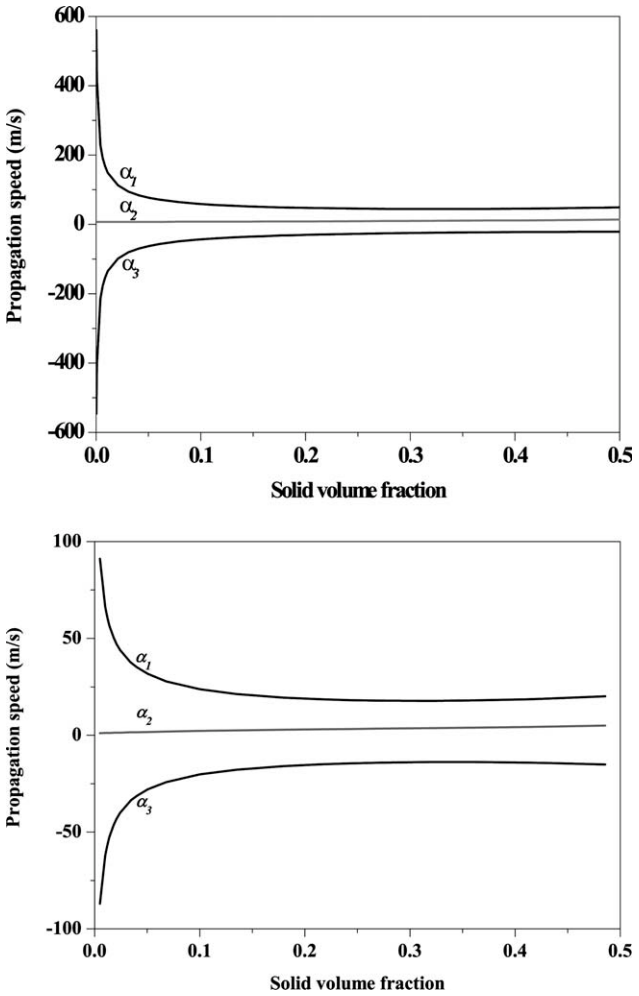

Figure 5. Lumped third-order compressible propagation speeds α_1, α_2 and α_3 in Eq. 27b, for (a) FCC and (b) Sand systems.

effect; the opposite is also true for $\varepsilon_{s0} > \varepsilon_{s0,IC}$. The values of $\varepsilon_{s0,IC}$ are shown in Table 2 for both systems. For the FCC catalyst-vapor system, it can be observed in Figure 2a, that the fluid compressibility consideration is far more important than the solid relaxation, due to its compressibility modulus, in most of the ε_{s0} interval. Nevertheless, both effects are important for the Sand-air system, as can be seen in Figure 2b. These behaviors are in agreement with the Stokes numbers for both systems; for FCC powders, the solid dynamics is highly dependent on the fluid dynamics but both dynamics become more independent for the Sand-air system.

Moreover, the coefficient values can be directly compared with the basic incompressible first-order wave whose coefficient is one. Thus, for an FCC system, the fluid compressibility significance is about 20% of the basic incompressible first-order wave, for a value of 0.5 for solid volume fraction; in contrast, the higher order incompressible behavior is only about a 0.3%. On the other hand, for the Sand system the fluid compressibility gives a maximum of about 10% of the basic behavior, while the higher order incompressible effect has an approximate maximum value of 5%. Therefore, both effects are significant for this system. Also, typical values of the local coefficient G' are in the range from 1.09 to 4.46 for FCC, and from 5.38 to 20.12 for the Sand system. The plot of the function $(C'G')$ shown in Figure 3, can be compared directly to the basic incompressible first-order behavior with the value one. This function accounts for gravity effects on the fluid compressibility and its importance is about 52% of the basic incompressible behavior for the Sand system and around 21% for the FCC powder, both for solid volume fractions close to 0.5.

Analysis of propagation speeds

In Figure 4, the basic propagation speed a, for an incompressible first-order wave for both systems is given, together with the higher order incompressible propagation speeds c_1 and c_2. Also the compressible incomplete second-order propagation speed η_{21} is given, which is in the same magnitude order than the previous ones. These velocities are ordered in the sequence $c_1 > \eta_{21} > a > c_2$ in both systems, even if the difference of η_{21} to a is very small for the FCC system.

The third-order propagation speeds α_1, α_2, and α_3, as shown in Eq. 27b, are dependent on the sound fluid propagation speed s and are expressed here by the sequence $\alpha_1 > \alpha_2 > \alpha_3$. They are found as the roots of the cubic equation (28) and are depicted in Figure 5, from $\varepsilon_{s0,min}$ up. The greatest and the lowest roots α_1 and α_3 can be directly associated to the acoustic wave propagation speeds[28] from a characteristic flow velocity, denoted in general as U_{flow}. These roots are given by

$$\tilde{\alpha}_1 = U_{flow} + s\sqrt{\frac{\rho_{g0}}{\varepsilon_0\left(\varepsilon_0\rho_{g0} + \varepsilon_{s0}\rho_{s0}\right)}}, \tag{46a}$$

$$\tilde{\alpha}_3 = U_{flow} - s\sqrt{\frac{\rho_{g0}}{\varepsilon_0\left(\varepsilon_0\rho_{g0} + \varepsilon_{s0}\rho_{s0}\right)}}. \tag{46b}$$

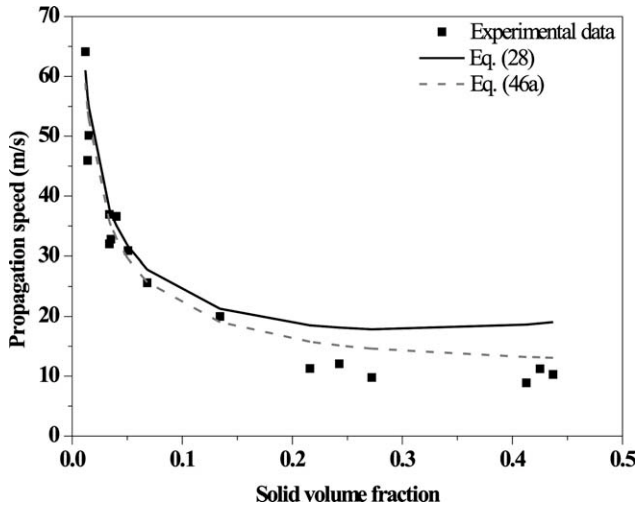

Figure 6. Pressure wave propagation speed for the Sand system. ■ Experimental data from van der Schaaf et al.[2] Continuous line: exact root of Eq. 28. Dash line: approximate solution, Eq. 46a with $U_{flow} = 0$.

Table 3. Percent Error of Pressure Wave Propagation Speeds for Best Approximations

Percent Error and System $\delta_j = 100\left\lvert\frac{\alpha_j - \tilde{\alpha}_j}{\alpha_j}\right\rvert$	Reference Value α_j/U_{flow} in Eq. 46a	Minimum Error	Maximum Error	Mean Square Error $E = \sqrt{\frac{\sum_{i=1}^{N} \delta_{j,i}^2}{N}}$
δ_1 for FCC	Exact root Eq. $28/U_m$	0.1	9.7	3.6
δ_3 for FCC	Exact root Eq. $28/U_m$	0.1	22.8	7.9
δ_1 for Sand	Exact root Eq. $28/U_m$	1.2	15.1	5.2
δ_3 for Sand	Exact root Eq. $28/U_m$	1.4	41.3	18.5
δ_1 for Sand	Experimental/$U_{\text{flow}} = 0$	0.4	48.8	23.4

The particular choice of the flow velocity U_{flow} to U_{m}, can be found in the literature[28] and gives better approximations than other choices to the exact roots of Eq. 28. However, for the Sand system the choice $U_{\text{flow}} = 0$ was the best one for the experimental results by van der Schaaf et al.[2] In Figure 6 the exact root α_1 of Eq. 28, as well as the approximated expression (46a) with $U_{\text{flow}} = 0$ is compared with the experimental values of the pressure wave propagation speed reported by van der Schaaf et al.[2] In Table 3, the mean square error of best approximations both to the exact root and to experimental values, are expressed as percentages, as well as the smallest and the greatest percent errors.

Whitham stability conditions

Evaluation of the propagation speeds showed that their order is in agreement to the stability criteria derived above; thus, the conditions $\alpha_1 > c_1 > \alpha_2 > c_2 > \alpha_3$ and $\alpha_1 > \eta_{21} > \alpha_2$ are fulfilled by both systems. Moreover, the lower limit of the wave number for linear stability κ_0, given by Eq. 42, is plotted for the FCC and the Sand systems in Figure 7.

In Eq. 44, the linear stability was considered as an extension to the study performed by Liu[19] on the basis of the incompressibility assumption. Therefore, it can be shown that the compressibility effect enhances the stability region, but only marginally, as could be seen by plotting the h_1 and h_2 functions. This criterion can be expressed as a percentage, by defining new dimensionless functions H_1 and H_2 as well as their equivalent criteria

$$H_1 = \frac{100h_1}{(c_1 - a)} = -\frac{100C}{(c_1 - a)s^2}\left({c_1}^3 - P_1{c_1}^2 + P_2c_1 - P_3\right) > -100, \tag{47}$$

$$H_2 = \frac{100h_2}{(a - c_2)} = \frac{100C}{(a - c_2)s^2}\left({c_2}^3 - P_1{c_2}^2 + P_2c_2 - P_3\right) > -100. \tag{48}$$

Plots of functions H_1 and H_2 are given in Figure 8, where the enhancement due to the compressibility effect is smaller than just a 0.01% for the FCC system and smaller than 0.03% for the Sand system.

Conclusions

In this work, linear waving structure in fast fluidized beds for both incompressible and compressible 1-D perturbation models was established. We showed that the incompressible model is embedded into the compressible one and becomes apparent in the limit $s \to \infty$. This model, expressed for volume fraction perturbations, has a typical second order waving structure, applied to a second-order spatial derivative of the pressure perturbations, and the compressible model is the sum of the same incompressible waving structure plus a compressible one. This last contribution consists of fourth, third, and a degenerate second-order wave operators, all of them multiplied by s^{-2}. However, the fourth-order wave is very small and can be neglected except for the solid volume

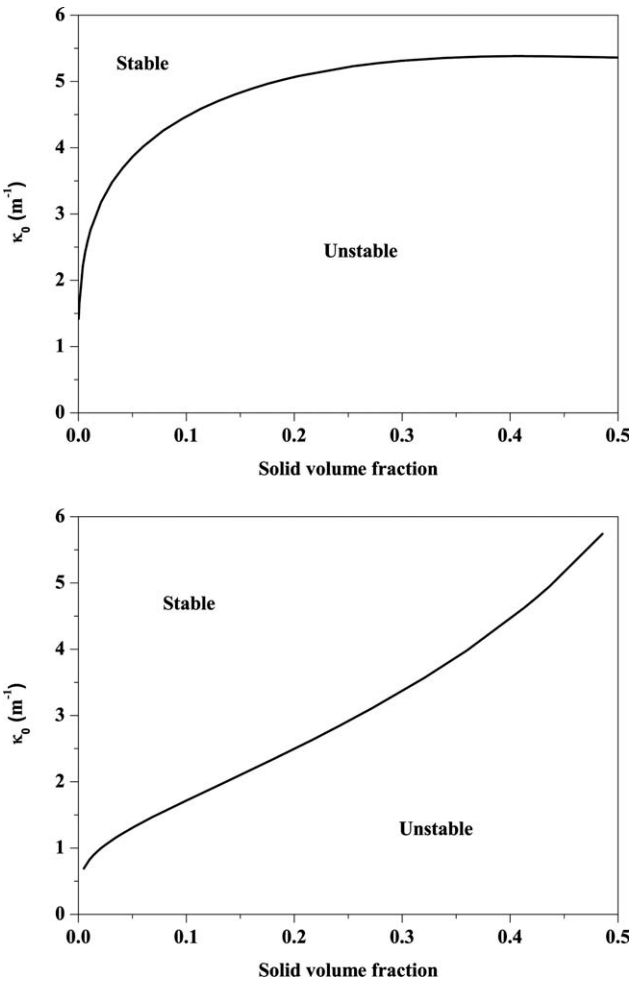

Figure 7. κ_0 for linear stability, as a function of ε_{s0} for (a) FCC and (b) Sand systems.

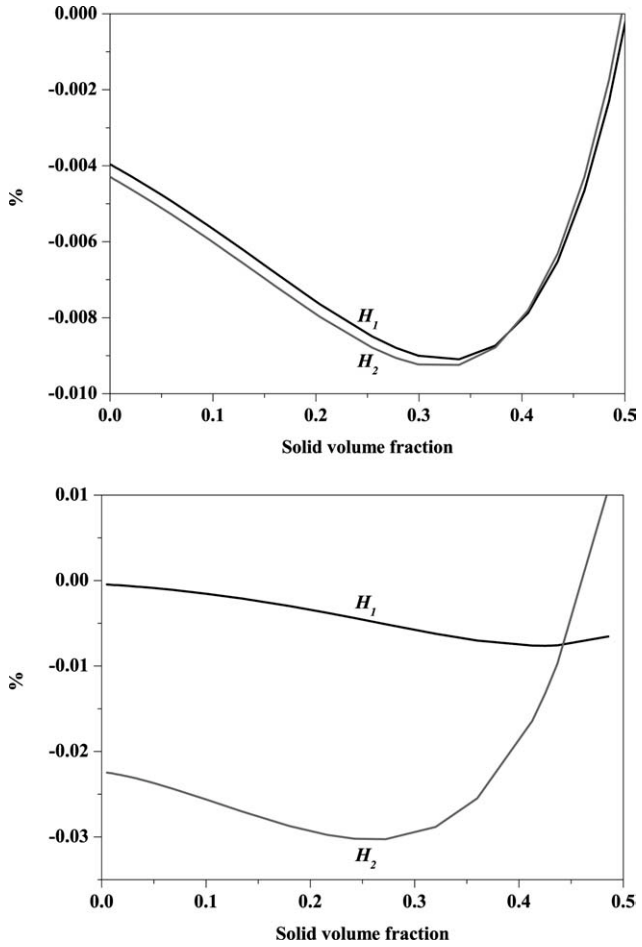

Figure 8. Broadening of the stability region due to fluid compressibility, expressed as percentages by functions H_1 and H_2 for (a) FCC system and (b) Sand system.

fractions smaller than a limit value $\varepsilon_{s0,min}$. The third-order compressible wave is of the same order of magnitude as the incompressible second order term, and the degenerate second order compressible term, which incorporates the effect of gravity, is about an order of magnitude greater than the third order one.

The model with explicit incompressible and compressible parts as given by Eq. 27a, can also be lumped to get an equivalent expression with just one differential operator for each order of derivatives, Eq. 27b. The second-order spatial derivative in the first-order wave of the incompressible operator, can be thought of as a degenerate waving structure, since it arises from the compressible third-order operator under the limit condition of the sound propagation speed becoming infinite.

A linear stability analysis based on the Whitham criterion on wave hierarchies was performed. It was shown that propagation speeds are ordered in such a way that $\alpha_1 > c_1 > \alpha_2 > c_2 > \alpha_3$ and $\alpha_1 > \eta_{21} > \alpha_2$. A criterion for the lower bound for the wave number κ_0 was also derived. Since the compressibility effect enhances the stability of the incompressible model, Liu's criterion was extended to involve the compressible part. Therefore, the compressibility effect could be estimated by extending the stability region, but rendering a negligible small effect on this extension.

The two particular systems selected for illustrating this assessment on the compressibility effect were an FCC catalyst-water vapor system and a Sand-air system. Their behavior is very different since their solid properties differ widely. The FCC system is mainly driven by the fluid, while the heavier solid particles in the Sand system behave more independently.

All these features show a greater influence of gas compressibility for the FCC, expressed in the incompressible second-order term by a large third-order wave coefficient and a negligibly small relaxation time. In contrast, for small solid volume fractions the relaxation time in the Sand system is one order of magnitude greater than the FCC. In this case, the compressible third-order coefficient is just half of the FCC one and the coefficient of the gravity effect on the gas compressibility term is more than twice important.

The behavior of the propagation speeds is affected by differences in the FCC and Sand dynamics. For FCC a is located in the middle of c_1 and c_2 while for Sand, a shift of c_1 and c_2 towards smaller and even negative values, renders a noncentral location of a. The pressure waves α_1 and α_3, in the limit $\varepsilon_{s0} \rightarrow 0$, become numerically coincident to the fluid sound propagation speed. Moreover, α_3 is near to the experimental pressure propagation speed in the whole ε_{s0} interval and the best fitting is reached when $U_{flow} = 0$.

Moreover, both systems are linearly stable according to the Whitham criterion, since the propagation speeds are ordered and satisfy a decreasing condition without overlapping. The minimum wave number to achieve stability gave a function roughly going from 1 to 6 m^{-1}, for very different intermediate values in the studied ε_{s0} interval.

Finally, it is very important to stress that the fluid compressibility effect is, at least as important as the effect of the solid compressibility modulus on the modeling strategy. Also, the gravity force on the gas compressibility interaction effect appears with the shape of a degenerate second-order wave with just one finite propagation speed η_{21}.

Acknowledgments

The authors highly acknowledge the Consejo Nacional de Ciencia y Tecnología (CONACyT), Mexico, for financial support through Grant CB-2005-C01-50379-Y and 162476 Scholarship for one of them (JRGSL). The authors gratefully acknowledge Prof. R.F. Rodríguez for useful comments on the manuscript.

Literature Cited

1. Gidaspow D. *Multiphase Flow and Fluidization: Continuum and Kinetic Theory Descriptions*. San Diego, California: Academic Press, Inc., 1994.
2. van der Schaaf J, Schouten JC, van den Bleek CM. Origin, propagation and attenuation of pressure waves in gas-solid fluidized beds. *Powder Technol*. 1998;95:220–233.
3. De Wilde J, Constales D, Heynderickx GJ, Marin GB. Assessment of filtered gas-solid momentum transfer models via a linear wave propagation speed test. *Int J Multiphase Flow*. 2007;33:616–637.
4. Bi HT, Grace JR, Zhu J. Propagation of pressure waves and forced oscillations in gas-solid fluidized beds and their influence on diagnostics of local hydrodynamics. *Powder Technol*. 1995;82:239–253.
5. Musmarra D, Poletto M, Vaccaro S, Clift R. Dynamic waves in fluidized-beds. *Powder Technol*. 1995;82:255–268.

6. Wallis GB. *One-Dimensional Two-Phase Flow*. New York: McGraw-Hill, Inc., 1969.
7. Gregor W, Rumpf H. Attenuation of sound in gas-solid suspensions. *Powder Technol*. 1976;15:43–51.
8. Atkinson CM, Kytömaa HK. Acoustic-wave speed and attenuation in suspensions. *Int J Multiphase Flow*. 1992;18:577–592.
9. Jones AV, Prosperetti A. The linear stability of general two-phase flow models-II. *Int J Multiphase Flow*. 1987;13:161–171.
10. Song JH, Ishii M. The well-posedness of incompressible one-dimensional two-fluid model. *Int J Heat Mass Transfer*. 2000;43:2221–2231.
11. Bi HT. A critical review of the complex pressure fluctuation phenomenon in gas-solids fluidized beds. *Chem Eng Sci*. 2007;62:3473–3493.
12. Ryzhkov AF, Tolmachev EM. Selection of optimal height for vibro-fluidized bed. *Teor Osn Khim Tekhnol*. 1983;17:140–147 [Theor Found Chem Eng (Engl. Transl.)].
13. Weir GJ. Sound speed and attenuation in dense, non-cohesive air-granular systems. *Chem Eng Sci*. 2001;56:3699–3717.
14. Needham DJ, Merkin JH. A note on the stability and the bifurcation to periodic solutions for wave-hierarchy problems with dissipation. *Acta Mechanica*. 1984;54:75–85.
15. Needham DJ, Merkin JH. The existence and stability of quasi-steady periodic voidage waves in a fluidized bed. *Zeitschrift für Angewandte Mathematik und Physik (ZAMP)*. 1986;37:322–339.
16. Göz MF. On the origin of wave patterns in fluidized beds. *J Fluid Mech*. 1992;240:379–404.
17. Soria A, Sánchez-López JRG, Salinas-Rodríguez EM. The incompressibility assumption assessment in fast fluidized bed wave propagation. *Proceedings of the 14th WASCOM Conference, Singapore, 2008:530–535*.
18. Ransom VH, Hicks DL. Hyperbolic two-pressure models for two-phase flow. *J Comput Phys*. 1984;53:124–151.
19. Liu JTC. Note on a wave-hierarchy interpretation of fluidized bed instabilities. *Proc R Soc Lond A*. 1982;380:229–239.
20. Whitham GB. *Linear and Nonlinear Waves*. New York: Wiley, 1974.
21. Drew DA. Mathematical modeling of two-phase flow. *Annu Rev Fluid Mech*. 1983;15:261–291.
22. Soria A, de Lasa HI. Averaged transport equations for multiphase systems with interfacial effects. *Chem Eng Sci*. 1991;46:2093–2111.
23. Sánchez-López JRG. MS Thesis. Waving phenomena on fast fluidization regime in a riser with compressibility effects. UAM-Iztapalapa, Mexico, 2003 [in Spanish].
24. Jackson R. *Hydrodynamic stability of fluid-particle systems*. In: Davidson JF, Clift R, Harrison D, editors. *Fluidization*, 2nd ed. Academic Press, Inc., 1985:47–72.
25. Homsy GM, El-Kaissy MM, Didwinia A. Instability waves and the origin of bubbles in fluidized beds-II Comparison with theory. *Int J Multiphase Flow*. 1980;6:305–318.
26. Kellogg Company MW. *Salina Cruz Oaxaca Refinery, catalytic plant operation manual*. Mexico: The Kellogg Company Pullman Incorporated, 1981 [in Spanish].
27. Jiradilok V, Gidaspow D, Damronglerd S, Koves WJ, Mostofi R. Kinetic theory based CFD simulation of turbulent fluidization of FCC particles in a riser. *Chem Eng Sci*. 2006;61:5544–5559.
28. Gregor W, Rumpf H. Velocity of sound in two-phase media. *Int J Multiphase Flow*. 1975;1:753–769.

Appendix A: Explicit Expressions of Matrices B, C, and D Given in Eq. 6

$$\mathbf{B}=\begin{pmatrix} b_{11} & b_{12} & 0 & 0 \\ b_{21} & 0 & 0 & 0 \\ 0 & 0 & b_{33} & 0 \\ 0 & 0 & 0 & b_{44} \end{pmatrix} \quad \mathbf{C}=\begin{pmatrix} c_{11} & c_{12} & c_{13} & 0 \\ c_{21} & 0 & 0 & c_{24} \\ 0 & c_{32} & c_{33} & 0 \\ c_{41} & c_{42} & 0 & c_{44} \end{pmatrix}$$

$$\mathbf{D}=\begin{pmatrix} 0 & 0 & 0 & 0 \\ 0 & 0 & 0 & 0 \\ d_{31} & d_{32} & d_{33} & d_{34} \\ d_{41} & d_{42} & d_{43} & d_{44} \end{pmatrix},$$

where the coefficients are defined in Table A1, with $\frac{dp_g}{d\rho_g}=s^2$.

Appendix B: Equation Systems Whose Roots are the Propagation Speeds

Incompressible second-order system

$$c_1+c_2=2\frac{(1-\varepsilon_0)\rho_{g0}v_{g0}+\varepsilon_0\rho_{s0}v_{s0}}{(1-\varepsilon_0)\rho_{g0}+\varepsilon_0\rho_{s0}}=p_1 \tag{B.01}$$

$$c_1c_2=\frac{(1-\varepsilon_0)\rho_{g0}{v_{g0}}^2+\varepsilon_0\rho_{s0}{v_{s0}}^2-\varepsilon_0(1-\varepsilon_0)\Phi_0'}{(1-\varepsilon_0)\rho_{g0}+\varepsilon_0\rho_{s0}}=p_2. \tag{B.02}$$

Combination of (B.01) and (B.02) gives the equation $c^2-p_1c+p_2=0$ whose roots are given by Eq. 21.

Compressible fourth-order system

$$\eta_{44}+\eta_{43}+\eta_{42}+\eta_{41}=2\left(v_{g0}+v_{s0}\right) \tag{B.03}$$

$$\eta_{44}\eta_{41}+\eta_{43}\eta_{41}+\eta_{44}\eta_{43}+\eta_{44}\eta_{42}+\eta_{43}\eta_{42}+\eta_{42}\eta_{41}=\frac{\rho_{s0}\left({v_{g0}}^2+4v_{g0}v_{s0}+{v_{s0}}^2\right)-(1-\varepsilon_0)\Phi_0'}{\rho_{s0}} \tag{B.04}$$

$$\eta_{44}\eta_{43}\eta_{42}+\eta_{44}\eta_{43}\eta_{41}+\eta_{44}\eta_{42}\eta_{41}+\eta_{43}\eta_{42}\eta_{41}=2\frac{\rho_{s0}v_{s0}\left(v_{g0}+v_{s0}\right)-(1-\varepsilon_0)\Phi_0'}{\rho_{s0}}v_{g0} \tag{B.05}$$

$$\eta_{44}\eta_{43}\eta_{42}\eta_{41}=\frac{\rho_{s0}{v_{s0}}^2-(1-\varepsilon_0)\Phi_0'}{\rho_{s0}}{v_{g0}}^2, \tag{B.06}$$

whose roots are given by Eqs. 24.

Compressible third-order system

$$\eta_{33}+\eta_{32}+\eta_{31}=P_1 \tag{B.07}$$

$$\eta_{33}\eta_{31}+\eta_{33}\eta_{32}+\eta_{32}\eta_{31}=P_2 \tag{B.08}$$

$$\eta_{33}\eta_{32}\eta_{31}=P_3 \tag{B.09}$$

where the polynomials P_k, $k=1,2,3$ are respectively.

Table A1. Nonvanish Coefficients of the Matrices B, C, and D

b_{ij}	c_{ij}	d_{ij}
$b_{11}=\rho_{g0}$	$c_{11}=\rho_{g0}v_{g0}$	$d_{31}=\beta\ (\varepsilon_{s0}-\varepsilon_0)\ (v_{g0}-v_{s0})$
$b_{12}=\varepsilon_0 s^{-2}$	$c_{12}=\varepsilon_0 v_{g0}s^{-2}$	$d_{32}=gp_0{}^{-1}\rho_{g0}(p_0)$
$b_{21}=-\rho_{s0}$	$c_{13}=\varepsilon_0\rho_{g0}$	$d_{33}=\beta\varepsilon_{s0}\varepsilon_0$
$b_{33}=\varepsilon_0\rho_{g0}$	$c_{21}=-\rho_{s0}v_{s0}$	$d_{34}=-\beta\varepsilon_{s0}\varepsilon_0$
$b_{44}=\varepsilon_{s0}\rho_{s0}$	$c_{24}=\varepsilon_{s0}\rho_{s0}$	$d_{41}=-\ [\beta(\varepsilon_{s0}-\varepsilon_0)\ (v_{g0}-v_{s0})+(\rho_{s0}-\rho_{g0})g]$
	$c_{32}=\varepsilon_0$	$d_{42}=-\varepsilon_{s0}gp_0{}^{-1}\rho_{g0}(p_0)$
	$c_{33}=\varepsilon_0\ \rho_{g0}v_{g0}$	$d_{43}=-\beta\varepsilon_{s0}\varepsilon_0$
	$c_{41}=-\ \varepsilon_{s0}\Phi_0'$	$d_{44}=\beta\varepsilon_{s0}\varepsilon_0$
	$c_{42}=\varepsilon_{s0}$	
	$c_{44}=\varepsilon_{s0}\rho_{s0}v_{s0}$	

$$P_1 = \frac{\varepsilon_0(4\varepsilon_0 - 1)v_{g0} + \varepsilon_0(1-\varepsilon_0)v_{s0} + \varepsilon_0(1-\varepsilon_0)\frac{\rho_{s0}}{\rho_{g0}}\left(v_{g0} + 2v_{s0}\right) + \left(\rho_{g0} - (1+\varepsilon_0)\rho_{s0}\right)\frac{g}{\beta}}{{\varepsilon_0}^2 + \varepsilon_0(1-\varepsilon_0)\frac{\rho_{s0}}{\rho_{g0}}} \tag{B.10}$$

$$P_2 = \frac{\left[\begin{array}{c}\varepsilon_0(5\varepsilon_0 - 2)v_{g0}^2 + 2\varepsilon_0(1-\varepsilon_0)v_{g0}v_{s0} + \varepsilon_0(1-\varepsilon_0)\frac{\rho_{s0}}{\rho_{g0}}v_{s0}\left(2v_{g0} + v_{s0}\right) \\ -2\left(\rho_{s0}v_{s0} - \rho_{g0}v_{g0} + \varepsilon_0\rho_{s0}v_{g0}\right)\frac{g}{\beta} - \frac{\varepsilon_0(1-\varepsilon_0)^2}{\rho_{g0}}\Phi_0'\end{array}\right]}{{\varepsilon_0}^2 + \varepsilon_0(1-\varepsilon_0)\frac{\rho_{s0}}{\rho_{g0}}} \tag{B.11}$$

$$P_3 = \frac{\left[\begin{array}{c}\varepsilon_0(2\varepsilon_0 - 1)v_{g0}^3 + \varepsilon_0(1-\varepsilon_0)v_{g0}^2v_{s0} + \varepsilon_0(1-\varepsilon_0)\frac{\rho_{s0}}{\rho_{g0}}v_{g0}v_{s_0}^2 \\ -\frac{\varepsilon_0(1-\varepsilon_0)^2}{\rho_{g0}}v_{g0}\Phi_0' + \left[(1-\varepsilon_0)\Phi_0' - \rho_{s0}v_{s0}^2 - \left(\varepsilon_0\rho_{s0} - \rho_{g0}\right)v_{g0}^2\right]\frac{g}{\beta}\end{array}\right]}{{\varepsilon_0}^2 + \varepsilon_0(1-\varepsilon_0)\frac{\rho_{s0}}{\rho_{g0}}} \tag{B.12}$$

and whose values are the roots $(\eta_{31},\eta_{32},\eta_{33})$ of the cubic equation

$$\eta^3 - P_1\eta^2 + P_2\eta - P_3 = 0. \tag{B.13}$$

Whole behavior (compressible and incompressible effects) third-order system

$$\alpha_1 + \alpha_2 + \alpha_3 = P_1 \tag{B.14}$$

$$\alpha_1\alpha_2 + \alpha_2\alpha_3 + \alpha_3\alpha_1 = P_2 - \frac{s^2}{C} \tag{B.15}$$

$$\alpha_1\alpha_2\alpha_3 = P_3 - \frac{s^2 a}{C} \tag{B.16}$$

whose values are the roots $(\alpha_1,\alpha_2,\alpha_3)$ of the cubic equation (28).

Manuscript received July 15, 2010, and revision received Nov. 30, 2010.